fluids

MDPI

Article

Self-Preservation of Turbulence Statistics in the Wall-Wake Flow of a Bed-Mounted Horizontal Pipe

Kalpana Devi [1], Prashanth Reddy Hanmaiahgari [1,*], Ram Balachandar [2] and Jaan H. Pu [3,*]

[1] Department of Civil Engineering, IIT Kharagpur, Kharagpur 721302, India; kalpanarajpoot@iitkgp.ac.in
[2] Department of Civil and Environmental Engineering, University of Windsor, Windsor, ON N9B 3P4, Canada; rambala@uwindsor.ca
[3] Faculty of Engineering and Informatics, School of Engineering, University of Bradford, Bradford BD7 1DP, UK
* Correspondence: hpr@civil.iitkgp.ac.in (P.R.H.); j.h.pu1@bradford.ac.uk (J.H.P.)

Abstract: This research article analyzed the self-preserving behaviour of wall-wake region of a circular pipe mounted horizontally over a flat rigid sand bed in a shallow flow in terms of mean velocity, RSS, and turbulence intensities. The study aims to investigate self-preservation using appropriate length and velocity scales.in addition to that wall-normal distributions of the third-order correlations along the streamwise direction in the wake region are analyzed. An ADV probe was used to record the three-dimensional instantaneous velocities for four different hydraulic and physical conditions corresponding to four cylinder Reynolds numbers. The results revealed that the streamwise velocity deficits, RSS deficits, and turbulence intensities deficits distributions displayed good collapse on a narrow band when they were non-dimensionalized by their respective maximum deficits. The wall-normal distance was non-dimensionalized by the half velocity profile width for velocity distributions, while the half RSS profile width was used in the case of the RSS deficits and turbulence intensities deficits distributions. The results indicate the self-preserving nature of streamwise velocity, RSS, and turbulence intensities in the wall-wake region of the pipe. The third-order correlations distributions indicate that sweep is the dominant bursting event in the near-bed zone. At the same time, ejection is the dominant bursting event in the region above the cylinder height.

Keywords: self-preservation in wall-wake; circular pipe; velocity deficit; RSS deficit; turbulence intensities deficit; third-order correlations

Citation: Devi, K.; Hanmaiahgari, P.R.; Balachandar, R.; Pu, J.H. Self-Preservation of Turbulence Statistics in the Wall-Wake Flow of a Bed-Mounted Horizontal Pipe. *Fluids* **2021**, *6*, 453. https://doi.org/10.3390/fluids6120453

Academic Editor: Rob Poole

Received: 17 September 2021
Accepted: 23 November 2021
Published: 14 December 2021

1. Introduction

The wake phenomenon is widespread in the nature, and its prevalent examples are environmental flows and flows occurring in many engineering applications. The wake is the highly turbulent region behind the bodies laid on the flat surfaces formed due to flow separation. The turbulent properties of the cylinder wake are a well-researched topic in fluid dynamics. Many investigations are available in the past literature [1–7] to study the cylinder wake. Djeridi et al. [1] conducted experimental research to explore the turbulent characteristics in the flow field of a circular cylinder in the near-bed upstream and near-wake region for a high value of Reynolds number equal to 14,000. They also analyzed the mean and turbulent flow field for a moderate blockage and an aspect ratio. Konstantinidis et al. [2] experimentally determined the mean and fluctuating velocity fields in the near wake of a circular cylinder under periodic velocity fluctuations incident on the mean flow. They described the wake in terms of the recirculation region, vortex formation region, the maximum intensity of velocity fluctuations, and vortex street's wavelength. Braza et al. [3] studied the flow field of a circular cylinder with a high blockage and a low aspect ratio. The flow field was explored in the starting point of the critical flow regime for a Reynolds number of 14,000. Akoz [4] experimentally estimated the characteristics of flow structures behind the cylinder, instantaneous and time-averaged velocity field, vorticity contours, streamline topology, and Reynolds stress concentrations for the cylinder Reynolds

number, Re_D between 1000 and 7000. They dictated separation point from the cylinder surface and the variation of length of the primary and secondary downstream separation regions with Reynolds numbers. Akoz and Kirkgoz [5] investigated the turbulent flow field of a bed-mounted horizontal cylinder for Reynolds numbers between 1000 and 7000. Devi and Hanmaiahgari [6] experimentally analyzed a wall-mounted cylinder's mean and turbulent characteristics at a downstream location. Devi et al. [7] conducted a comparative study for the flow field of a wall-mounted cylinder to determine the effect of gravel-bed roughness compared to sand bed roughness. Despite numerous research in this field, many issues related to the cylinder wake are still unresolved, especially in shallow flows.

In the shallow flows, the horizontal length scale is generally larger than the wall-normal length scale [8]. Destabilizing shallow flows are caused by an abrupt change in topology, such as a bluff body over a flat surface, resulted in shallow wakes. Many researchers [9–11] have studied the nature of shallow wakes. Akilli and Rockwell [11] used flow visualization techniques in addition to particle image velocimetry (PIV) to study the shallow flows in the near wake region of a circular cylinder. They discussed the variation of mean velocity, Reynolds stress, vorticity, and streamline topology at three different wall-normal distances. The channel bed can significantly affect the flow characteristics of the shallow wake, and bed effects are attenuated while moving away from it towards the free surface. In the near-bed region of the flow, the bed restricts the development of the wake, diminishes the interaction between shear layers, and stabilizes the flow [12].

Self-preservation of turbulent wakes downstream of a cylinder at high Reynolds numbers was initially reported by Townsend [13,14] in his elaborate investigations. Out of these wakes, the one which frequently occurs in the environment is the shallow wake. The concept of self-preservation of turbulent flows is also known as local similarity or self-similarity. If some or all statistical characteristics of a turbulent flow are a function of only scales, the flow is called self-preserving in its behaviour. In other words, a turbulent flow in its self-preserving condition is the only function of its length and velocity scales. The far-field of a turbulent free shear layer such as a wake and a jet are classic examples of self-preserving flows. Maji et al. [15] reviewed the occurrence of von Kármán vortex streets as a function of solid volume fraction in the wake region of a group of wall-mounted vertical cylinders. Sadeque et al. [16] analyzed the flow patterns of the near-wakes of the wall-mounted vertical cylinder in the turbulent shallow flow. They found that flow fields in the region away from the wall are similar. They also perceived that the turbulent kinetic energy and the primary Reynolds stress distributions displayed the self-preserving behaviour in moderate to deeply submerged cylinders. Balachandar et al. [8] and Tachie and Balachandar [17] deduced that even in a near-wake region of the flow, the self-preserving characteristics can be established in terms of the time-averaged velocity distributions by using appropriate velocity and length scales. Maji et al. [18] analyzed the self-preserving behaviour in the interior and the wake region of the vegetation patch regarding the mean flow velocities in the streamwise and wall-normal directions and turbulence intensities, RSS, and turbulent kinetic energy (TKE). They observed that the time-averaged streamwise velocity distributions depict self-preserving characteristics for both emergent and sparse vegetation patches in their outer, interior, and wake regions when scaled by their depth-averaged value. The self-preserving behaviour of the time-averaged streamwise velocity distributions was independent of the aspect ratios and the Reynolds numbers. Similar observations were also made for the RSS profiles. In the past literature [8,16,17], different velocity and length scales were used for velocity, RSS, and turbulence intensities distributions. Balachandar et al. [8] and Tachie and Balachandar [17] used $U_{max} - U_{min}$ as a velocity scale and b as a length scale for the velocity distributions to establish the self-preserving characteristics of the wake region of a sharp-edged plate. Here, U_{max} and U_{min} are the maximum and the minimum velocities, respectively, in the wake region at a particular streamwise distance, x/D, and b is the wall-normal distance at which $U - U_{min}$ is equal to one half of the $U_{max} - U_{min}$. Sadeque et al. [16] used U_{1m} as the velocity scale for velocity profiles for the bed-mounted cylinder. In their study, the U_{1m} is equivalent to

$U_{max} - U_{min}$ of Balachandar et al. [8] and Tachie and Balachandar [17]. They also observed an excellent collapse of the velocity profiles in the near wake region of the cylinder. The velocity deficit profiles collapse on a narrow band for this scaling, representing that the wall-wake region of the pipe is self-preserving in nature. Despite that much research in this area, there are very few studies that explore the self-preserving characteristics of the wall-wake region of a bed-mounted horizontal circular pipe in the shallow flow with proper scaling for the velocity, RSS, and turbulence intensities.

Therefore, the main objective of this study is to assess the self-preserving characteristics of the wall-wake flow of a bed-mounted circular pipe in terms of streamwise velocity, RSS, and turbulence intensities for different inflow conditions. Further, the variation of the wall-normal distributions of third-order correlations along the streamwise direction in the wake region was also evaluated. For this purpose, an ADV probe was used to measure instantaneous three-dimensional (3D) velocity data. After post-processing the velocity data, it was used to determine turbulence statistics of the flow and their deficits and maximum values. Henceforth, how the wall-normal profiles of the time-averaged streamwise velocity u^+, RSS ${\tau_{uw}}^+$, streamwise turbulence intensity ${\sigma_u}^+$, wall-normal turbulence intensity ${\sigma_w}^+$ in non-dimensional forms and third-order correlations M_{jk} change in the wake region of the pipe with streamwise distance, $\hat{x}$ were also documented. Additionally, the wall-normal distributions of non-dimensional velocity deficit $\Delta u/(\Delta u)_{max}$, non-dimensional RSS deficit $\Delta\tau_{uw}/(\Delta\tau_{uw})_{max}$, non-dimensional streamwise turbulence intensity deficit $\Delta\sigma_u/(\Delta\sigma_u)_{max}$ and non-dimensional wall-normal turbulence intensity deficit $\Delta\sigma_w/(\Delta\sigma_w)_{max}$ were investigated to determine the self-preserving behaviour of velocity, RSS, and turbulence intensities, respectively. Besides this, the decay of maximum velocity deficit $(\Delta u)_{max}/u_*$, maximum RSS deficit $-(\Delta\tau_{uw})_{max}/{u_*}^2$, maximum streamwise turbulence intensities deficit $-(\Delta\sigma_u)_{max}/u_*$ and maximum wall-normal turbulence intensities deficit $-(\Delta\sigma_w)_{max}/u_*$ with streamwise distance, $\hat{x}$ were also evaluated. This was followed by the analysis of the streamwise growth of half velocity profile width, z_1 and half RSS profile width, z_2.

2. Experimental Setup and Data Measurement Procedure

This section presents the experimental channel description, sand bed material analysis, pipe model details, ADV probe specifications, a summary of the hydraulic and physical conditions of experimental runs, data measurement procedure, and data processing techniques used.

2.1. Experimental Setup

A rectangular closed-loop channel of 12 m length with a cross-section of $B \times H = 0.91$ m $\times$ 0.70 m was utilized for the experimental purpose [6,7]. A constant streamwise bed slope of 0.23% was maintained along the channel length for all the experimental runs. The channel side walls at the test section consisted of transparent glass to facilitate visualization. At the channel inlet, two flow straighteners were provided to suppress the pump vibrations. A circular pipe of diameter D was laid on the bed at a distance of 6.5 m downstream of the channel inlet. The pipe was laid in such a way that it was not allowing the flow underneath it. Uniform sand having a median size, d_{50} equal to 2.54 mm, was coated over the bed to generate the rough surface. A user-configured tailgate was provided at the channel outlet to regulate the flow depth. The water surface levels were measured by employing two sets of Vernier point gauges with an accuracy of $\pm$0.1 mm. The ADV system was carried on a movable trolley supported on two rails over the channel walls.

The streamwise direction of the coordinate system used in the experiment is taken as the x-axis with the positive in the downstream direction and the negative in the upstream direction. The transverse direction is taken as the y-axis with the positive towards the left of the channel centerline and the negative on the right side of the central plane of the channel. The z-axis was oriented in the wall-normal direction to the channel bed with a positive in the vertically upward direction. The origin of the coordinate system was located at the intersection point of the axis of the pipe and the central wall-normal plane (xz).

A four-receivers down-looking ADV probe (Vectrino plus) manufactured by Nortek company (Nortek AS, Vangkroken 2, NO-1351 RUD, Norway), operating with an acoustic frequency of 10 MHz, was utilized to record 3D instantaneous velocity data. The Vectrino collect the velocity data at a location 5 cm below the transmitting probe. The sampling volume cylinder diameter and height both are 6 mm. The data were recorded for a sampling time equal to five minutes with a sampling frequency of 100 Hz. The sampling time of five minutes was found to be adequate for obtaining self-determining time-averaged flow velocities [19]. Unwanted spikes mostly corrupted the near-bed data; therefore, despiking was adopted to separate the noise from the raw data using the despiking techniques suggested by previous researchers [20–22], and replaced using a cubic interpolation method. To validate the quality of the data obtained after despiking, the signal-to-noise ratio (SNR) test as proposed by Chanson et al. [23] was implemented. The data threshold values of SNR and correlation coefficient as 17 and 70%, respectively, were maintained. The uncertainty statistics of the ADV probe were analyzed by collecting 10 samples at 10 mm above the bed level, for a sampling duration of 5 min at a sampling rate of 100 Hz. The uncertainties in the velocity terms, Reynolds stresses and turbulence intensities terms, and third-order correlations are less than 5%, 10%, and 13%, respectively.

2.2. Data Measurement Procedure

The channel was left unused for an hour to stabilize the flow after starting the pump. All data measurements were taken in the central wall-normal plane (xz) of the channel. Four experimental runs, namely, Run 1, Run 2, Run 3, and Run 4, were conducted corresponding to four different cylinder Reynolds numbers (Re_D). The summary of all four experimental runs is given in Table 1.

Table 1. The summary of all four experimental runs.

Exp. Run	D (m)	h (m)	U (m/s)	u_* (m/s)	F_r	Re_D
Run 1	0.05	0.3	0.15	0.0071	0.111	7500
Run 2	0.05	0.3	0.19	0.0092	0.111	9500
Run 3	0.08	0.3	0.15	0.0071	0.087	12,000
Run 4	0.08	0.3	0.19	0.0092	0.111	15,200

Two different pipe diameters, D of 5 and 8 cm, were used as pipe models. A constant flow depth, h of 0.3 m, was maintained for all four runs. Two approach flow area-averaged velocities, U of 0.15 and 0.19 m/s, were maintained during the complete experiment. The cylinder Reynolds number and the Froude number were estimated as $Re_D = UD/\nu$, and $F_r = U/\sqrt{gh}$, respectively. All experimental runs were conducted under subcritical flow conditions, as is clear from the value of F_r from Table 1. The approach flow shear velocity, u_* was determined by linearly extending the RSS profile to the channel bed [24].

The data were recorded at nine streamwise locations ($\hat{x} = -4$, 0, 2, 3, 4, 6, 8, 10, and 12) for each run. Here, $\hat{x}$ is the non-dimensional streamwise distance, taken as the ratio of streamwise distance, x to the pipe diameter, D and written as $\hat{x} = x/D$. The $\hat{x} = -4$ is an undisturbed upstream location, $\hat{x} = 0$ is located just above the pipe, and the rest of the data measurement locations are in the wake region of the pipe. For each measurement location, data were collected at 26 wall-normal points as z = 0.003, 0.005, 0.007, 0.009, 0.012, 0.015, 0.02, 0.025, 0.03, 0.035, 0.04, 0.045, 0.05, 0.06, 0.07, 0.08, 0.09, 0.1, 0.11, 0.13, 0.15, 0.17, 0.19, 0.21, 0.23 and 0.245 m except at $\hat{x} = 0$. At $\hat{x} = 0$, it was not feasible to record data below the top level of pipe, so z = 0.06 and 0.09 m onwards were collected for 5 cm and 8 cm diameter pipes, respectively. A schematic diagram of the experimental setup showing its plane view with the streamwise measurement locations for Run 1, Run 2, Run 3, and Run 4, along with the coordinate system used for the experiments, is shown in Figure 1.

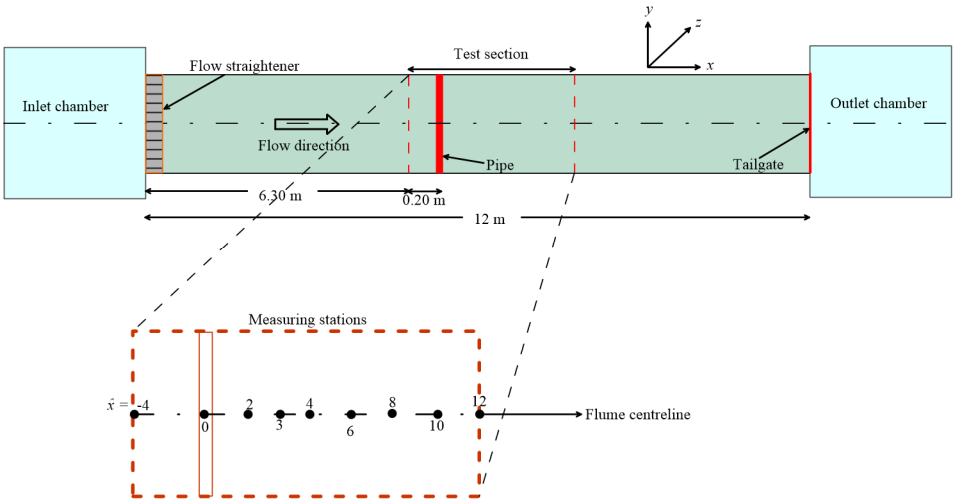

Figure 1. Schematic diagram of the experimental setup showing its plane view with the streamwise measurement locations for Run 1, Run 2, Run 3, and Run 4, and the coordinate system used for the experiments.

Figure 2 depicts the vector plots of the non-dimensional resultant velocity, U^+ along the non-dimensional central wall-normal plane, xz ($\hat{x}$, z/D) of the channel for Run 3 in the wall-wake region of the pipe. The diameter of pipe D was used as the streamwise length scale to non-dimensionalize streamwise distance, x as $\hat{x}(= x/D)$. The vector plots were shown only up to a wall-normal domain of $2D$ to depict the flow field in the near-bed region. The approach flow shear velocity, u_* is used as velocity scale to normalize the velocity vector of magnitude, $\overline{U} = \sqrt{\overline{u}^2 + \overline{w}^2}$ with the direction, $\theta = \tan^{-1}(\overline{w}/\overline{u})$. Here, θ is the angle made by the velocity vector with the horizontal direction. It was observed from Figure 2 that the flow separated at the top surface of the pipe and later reattached to the channel bed downstream with the formation of a recirculation region in the near-bed flow zone. The recirculation region is stretched up to $\hat{x} = 7.4$. Velocity vectors are pointed in the opposite direction of the flow in the recirculation region's near-bed zone, indicating the existence of the resultant negative velocity in the region. The dotted blue line demarcates the recirculation region in Figure 2. Beyond this line, the mean velocity becomes entirely positive. After the reattachment point, the flow starts becoming similar to its undisturbed upstream form. It is noteworthy that within the streamwise domain of $12D$, the mean velocity is not fully recovered to its undisturbed upstream value.

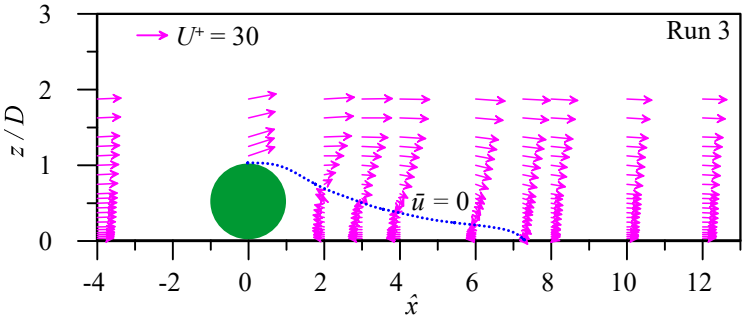

Figure 2. Vector plot of non-dimensional resultant velocity, U^+ along the central wall-normal plane (xz) of the channel for Run 3 in the wall-wake region of the pipe.

3. Results and Discussion

The approach flow shear velocity, u_*, was used as the velocity scale to non-dimensionalize the turbulent characteristics and the flow depth, h, was used as the wall-normal length scale for the wall-normal distance, z, as $\overline{z}$ $(= z/h)$. The wall-normal profiles of the non-dimensional time-averaged streamwise velocity, $u^+ (= \overline{u}/u_*)$, in the wake region of the pipe at a different streamwise distance, $\hat{x}$, for Run 3 and Run 4 are plotted in Figure 3. It is clear from Figure 3 that the streamwise velocity, u^+, has a negative sign in the near-bed region because of flow separation while it becomes positive in the region away from the bed. The velocity in the free-surface region is also affected by the presence of the pipe, and its magnitude is different from the corresponding approach flow velocity in the free surface region. The velocity in the free-surface region of the recirculation region is greater than the undisturbed upstream velocity at the same elevation because of lower near-bed velocities in the recirculation region which shows mass conservation. In addition, this result reveals that the flow was diverted upward and accelerated in the near-surface region due to the separation of the flow from the pipe. The maximum magnitude of the streamwise velocity is occurring near the free surface for all streamwise locations, $\hat{x}$. The maximum magnitude of the streamwise velocity is increasing along with streamwise distance up to $\hat{x} = 6$ and then decreasing with a further increase in $\hat{x}$. It is noteworthy that the negative velocity is fully recovered at a streamwise distance of $\hat{x} = 8$, in both the runs (Run 3 and Run 4). The velocity, u^+-, distributions in the wake region display an upward concavity in their profiles, and this asymmetric velocity distribution occurs due to the wall-wake effects.

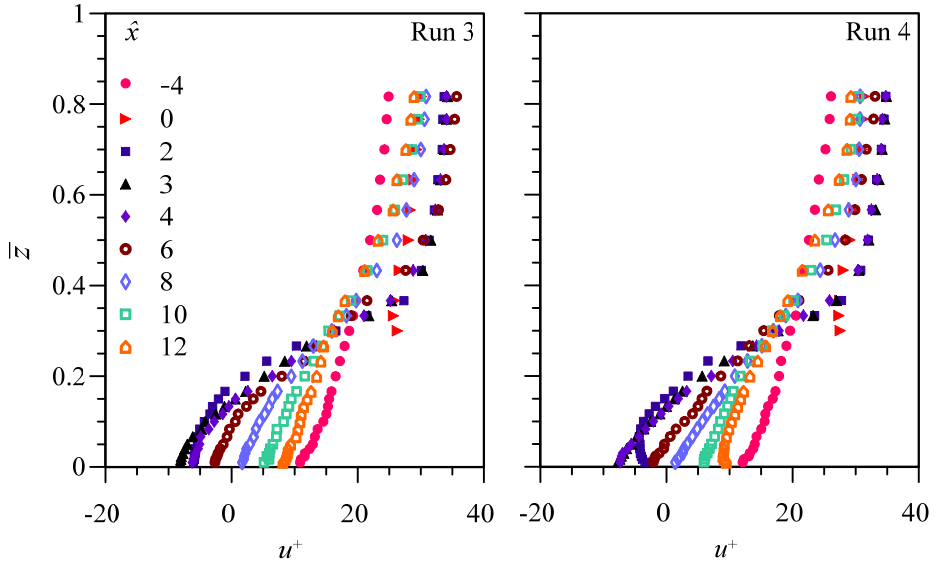

Figure 3. Wall-normal profiles of non-dimensional time-averaged streamwise velocity, u^+, in the wake region of the pipe at different streamwise locations, $\hat{x}$, for Run 3 and Run 4.

The points of inflection $(d^2\overline{u}/dz^2 = 0)$ in the individual u^+ profiles are observed near the top level of the pipe, $z/D \approx 1$. In the free-surface region, the velocity u^+- distributions are attaining almost the same velocity gradient, $d\overline{u}/dz$. The extrapolation of the streamwise velocity profiles up to the channel bed verified the preservation of the no-slip condition.

Figure 4 depicts the schematic diagram of a typical wall-normal distribution of streamwise velocity deficit, Δu, in the wall-wake region of the pipe along with the definition of the half velocity profile width, z_1. The velocity deficit, Δu, is the difference between the upstream undisturbed time-averaged streamwise velocity at particular elevation z and the downstream wall-wake time-averaged streamwise velocity at the same elevation. The velocity deficit, Δu (z), at a specific wall-normal distance, z, can be written as $\Delta u\ (z) = u_{u/s}(z) - u_{d/s}(z)$. Here, $u_{u/s}(z)$ is the upstream undisturbed time-averaged streamwise velocity at an elevation, z, while $u_{d/s}(z)$ is the downstream wall-wake time-

averaged streamwise velocity at the same elevation. The half velocity profile width, z_1, is the wall-normal elevation from the bed at which the velocity deficit is equal to one-half of the maximum velocity deficit, $(\Delta u)_{max}$.

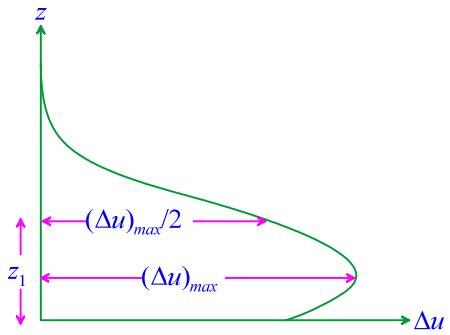

Figure 4. Schematic representation of a typical wall-normal distribution of streamwise velocity deficit, Δu, in the wall-wake region of the pipe along with the definition of the half velocity profile width, z_1.

Figure 5a displays the variation of $\Delta u/(\Delta u)_{max}$ against z/z_1 for Run 1, Run 2, Run 3, and Run 4 in the wall-wake region of the pipe, depicting the self-preserving characteristics of the velocity deficit, Δu, distributions. The maximum velocity deficit, $(\Delta u)_{max}$, is used as the velocity scale, and the half velocity profile width, z_1, is taken as the wall-normal length scale. The velocity deficit profile is exhibiting a single peak in its distribution at $z/z_1 \approx 0.25$. The self-preserving characteristics of the velocity deficit profiles are found to be independent of approach flow conditions and diameter of the cylinder, D. All of the streamwise velocity profiles are showing a good collapse over a narrow band for the wall-normal domain of the study, $z/D < 2$, and for the complete streamwise domain of the research. Above the wall-normal domain, $z/D > 2$ velocity profiles are not self-preserving in nature; therefore, they are excluded from the analysis. It can also be observed that the value of non-dimensional velocity deficit is equal to unity at $z/z_1 \approx 0.25$, which simply implied that $z \approx 0.25 z_1$ is the wall-normal location of the maximum velocity deficit, $(\Delta u)_{max}$.

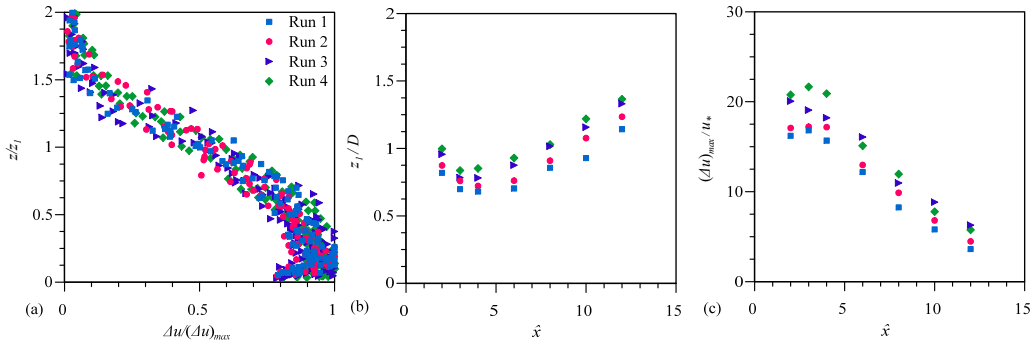

Figure 5. Self-preservation analysis of streamwise velocity distribution in the wall-wake region of the pipe for Run 1, Run 2, Run 3, and Run 4: (**a**) variation of $\Delta u/(\Delta u)_{max}$ against z/z_1, depicting the self-preservation in velocity deficit (Δu) distribution; (**b**) streamwise growth of non-dimensional half velocity profile width, z_1/D; and (**c**) streamwise decay of non-dimensional maximum velocity deficit, $(\Delta u)_{max}/u_*$.

Figure 5b portrays the streamwise growth of non-dimensional half velocity profile width, z_1/D for Run 1, Run 2, Run 3, and Run 4 in the wall-wake region of the pipe. The diameter of pipe D is used as the wall-normal length scale. It can be observed from Figure 5b that the half velocity profile width, z_1/D, grows consistently and gradually

except for starting two points. This variation in the half velocity profile width is resulting from an increase followed by a decrease in the thickness of the wake region downstream of the cylinder. A similar observation was also made by Tachie and Balachandar [17], with a slightly different value of streamwise distance as $\hat{x} \geq 5$, the half velocity profile width grows constantly and gradually with $\hat{x}$. Contrary to this, Sadeque et al. [16] found a constant decline in the half velocity profile width with streamwise distance for a bed-mounted vertical cylinder.

The streamwise decay of non-dimensional maximum velocity deficit, $(\Delta u)_{max}/u_*$, for Run 1, Run 2, Run 3, and Run 4 are demonstrated in Figure 5c. The approach flow shear velocity, u_*, is taken as the velocity scale to normalize the maximum velocity deficit, $(\Delta u)_{max}$. It is perceived from Figure 5c that the maximum velocity deficit, $(\Delta u)_{max}/u_*$, decays in the streamwise direction with $\hat{x}$. Its decay indicates the recovery of the wall-wake flow velocity similar to its undisturbed upstream values. The flow is uniformly and quickly recovering to its undisturbed upstream values. Schmeeckle and Nelson [16] also made similar observations.

The wall-normal profiles of the non-dimensional RSS, ${\tau_{uw}}^+$ in the wake region of the pipe at a different streamwise distance, $\hat{x}$, for Run 3 and Run 4 are shown in Figure 6. Here, Reynolds shear stress (RSS), τ_{uw} is expressed as $\tau_{uw} = -\overline{u'w'}$. It is visible from Figure 6 that RSS starts with a small positive value at the bed and increases sharply with an increase in the wall-normal distance, z. It attained its peak at the top level of the pipe ($z/D \approx 1$) and decreased quickly with a further rise in $\overline{z}$. Henceforth, the value of RSS becomes very small and almost invariant of the wall-normal distance, z in the free-surface region. The location of the peak of the RSS corresponds to the point of inflection ($d^2\overline{u}/dz^2 = 0$) in the velocity profiles. It is understood that the peaks in RSS at the top level of the pipe are caused by the enhanced mixing of turbulence at that level.

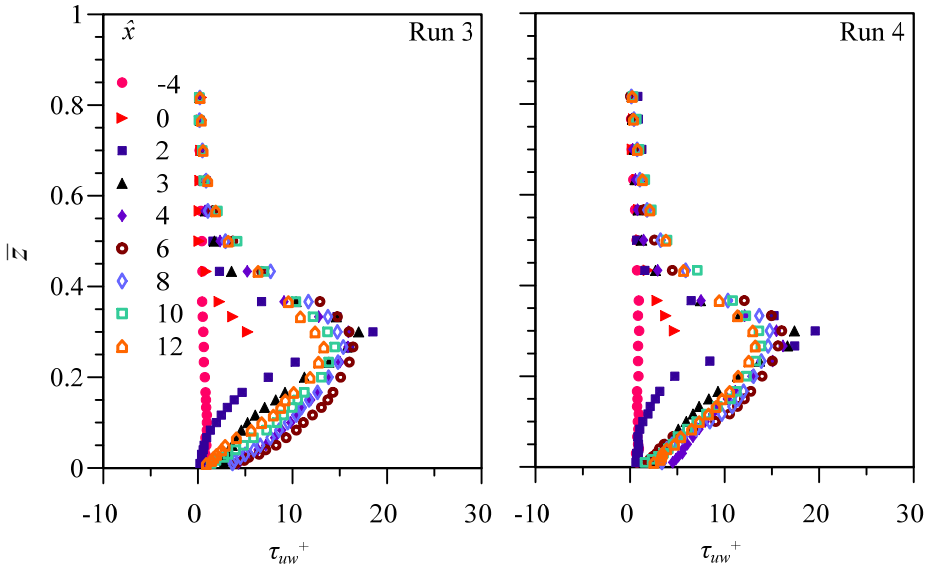

Figure 6. Wall-normal profiles of non-dimensional RSS, ${\tau_{uw}}^+$, in the wake region of the pipe at different streamwise locations, $\hat{x}$, for Run 3 and Run 4.

Figure 7 illustrates the diagram of the typical wall-normal distribution of RSS deficit, $\Delta\tau_{uw}$, in the wall-wake region of the pipe along with the definition of the half RSS profile width, z_2. The RSS deficit, $\Delta\tau_{uw}$, is the difference between the downstream wall-wake RSS at an elevation, z, and upstream undisturbed RSS at the same elevation. The RSS deficit, $\Delta\tau_{uw}(z)$, at a particular elevation, z, can be written as $\Delta\tau_{uw}\ (z) = \tau_{u/s}(z) - \tau_{d/s}(z)$. Here, $\tau_{u/s}(z)$ is the upstream undisturbed RSS at an elevation, z, and $\tau_{d/s}(z)$ is the downstream wall-wake RSS at the same elevation. The half RSS profile width, z_2, was estimated similarly

to the half velocity profile width, z_1. The half RSS profile width z_2 is the wall-normal height from the bed at which the RSS deficit is equal to $0.5(\Delta\tau_{uw})_{max}$.

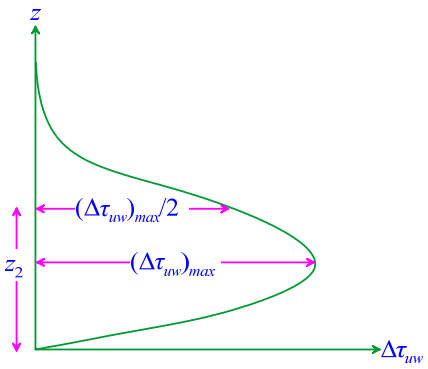

Figure 7. Schematic representation of a typical wall-normal distribution of RSS deficit, $\Delta\tau_{uw}$, distribution in the wall-wake region of the pipe along with the definition of the half RSS profile width, z_2.

Figure 8a expresses the variation of $\Delta\tau_{uw}/(\Delta\tau_{uw})_{max}$ against z/z_2 for Run 1, Run 2, Run 3, and Run 4 in the wall-wake region of the pipe, by depicting the self-preserving characteristics in the RSS deficit (Δu) profiles. The self-preservation of the wall-wake is evaluated based upon the collapse of the RSS deficit profiles on a narrow band. The maximum RSS deficit, $(\Delta\tau_{uw})_{max}$ is used as velocity scale and the half RSS profile width, z_2 is taken as the wall-normal length scale. The RSS deficit profiles are collapsing on a narrow band for this scaling, which demonstrates that the wall-wake region of the pipe is self-preserving in nature. The self-preserving characteristics of the RSS deficit profiles are found to be independent of the approach flow conditions similar to the velocity deficit profiles. Similar to velocity profiles, all RSS profiles show good collapse with the streamwise distance, $\hat{x}$, for the wall-normal domain of study, $z/D < 2$. It is noteworthy that the RSS deficit profiles display a single peak, and it occurs at $z/z_1 \approx 0.6$. It can also be observed from Figure 8a that the value of non-dimensional RSS deficit $(\Delta\tau_{uw})_{max}$ was equal to unity for $z/z_1 \approx 0.6$. It simply reveals the peak value of the RSS deficit occurs at $z \approx 0.6z_1$ i.e., $\Delta\tau_{uw}|_{z=0.6z_1} = (\Delta\tau_{uw})_{max}$.

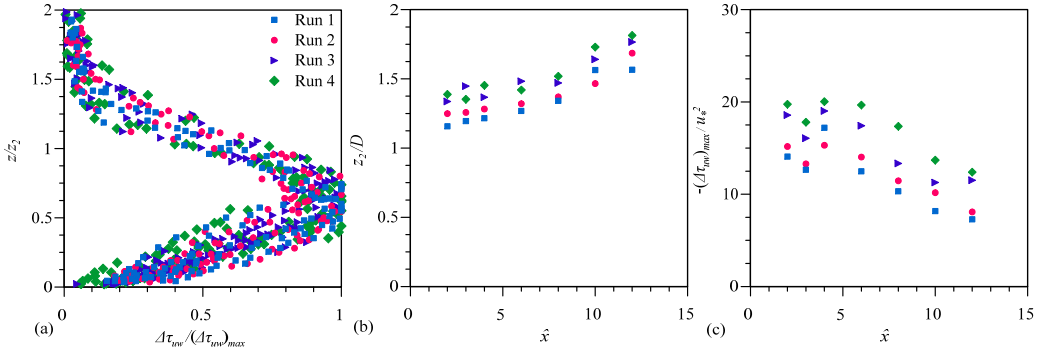

Figure 8. Self- preservation analysis of RSS distribution in the wall-wake region of the pipe for Run 1, Run 2, Run 3, and Run 4: (**a**) variation of $\Delta\tau_{uw}/(\Delta\tau_{uw})_{max}$ against z/z_2, depicting the self-preservation in RSS deficit ($\Delta\tau_{uw}$) distribution; (**b**) streamwise growth of non-dimensional half RSS profile width, z_2/D; and (**c**) streamwise decay of non-dimensional maximum RSS deficit,$-(\Delta\tau_{uw})_{max}/{u_*}^2$.

Figure 8b displays the streamwise growth of non-dimensional half RSS profile width, z_2/D, for Run 1, Run 2, Run 3, and Run 4 in the wall-wake region of the pipe. The diameter of the pipe, D, is used as the wall-normal length scale. It can be observed from Figure 8b

that half RSS profile width, z_2/D, grows in the streamwise direction with an increase in the streamwise distance, $\hat{x}$.

The streamwise decay of non-dimensional maximum RSS deficit, $-(\Delta\tau_{uw})_{max}/{u_*}^2$ for Run 1, Run 2, Run 3, and Run 4 are depicted in Figure 8c. The negative sign is used before the maximum RSS deficit $-(\Delta\tau_{uw})_{max}/{u_*}^2$, since $\tau_{d/s}(z)$ is greater than $\tau_{u/s}(z)$. The approach flow shear velocity, u_*, is taken as the velocity scale to normalized the maximum RSS deficit, $-(\Delta\tau_{uw})_{max}$. Figure 8c demonstrates that the maximum RSS deficit, $-(\Delta\tau_{uw})_{max}/{u_*}^2$, decays in the streamwise direction with $\hat{x}$, which indicates the recovery of the flow with an increase in $\hat{x}$. Similar results were also revealed by Sadeque et al. [16], although their case is of a bed-mounted vertical cylinder. These patterns in the variation of $-(\Delta\tau_{uw})_{max}/{u_*}^2$ in the streamwise direction are happening due to the dampening of the turbulence mixing with an increase in $\hat{x}$ and recovering the flow similar to its undisturbed upstream form.

The turbulence intensity downstream of the pipe exists due to the fluctuations in the instantaneous flow velocity influenced by the pipe and bed roughness. Non-dimensional turbulence intensities in the streamwise, ${\sigma_u}^+$ and wall-normal directions, ${\sigma_w}^+$ are given as ${\sigma_u}^+ = \sigma_u/u_*$ and ${\sigma_w}^+ = \sigma_w/u_*$, respectively. The streamwise, σ_u $\left(=\sqrt{\overline{u'u'}}\right)$ and wall-normal, σ_w $(=\sqrt{\overline{w'w'}})$ turbulence intensities are the root mean square (RMS) of the fluctuating velocity components in respective directions, representing the strength of turbulence. The wall-normal profiles of the non-dimensional streamwise, ${\sigma_u}^+$ and wall-normal turbulence intensities, ${\sigma_w}^+$ in the wake region of the pipe at a different streamwise distance, $\hat{x}$ for Run 3 and Run 4 are depicted in Figures 9 and 10. It is observed from Figures 9 and 10 that the wall-normal distributions of turbulence intensities are akin to RSS distribution with smaller magnitudes. Similar to RSS distributions, at the bed, ${\sigma_u}^+$ and ${\sigma_w}^+$ for both runs, are starting with small positive values, and increasing sharply with an increase in $\overline{z}$ until they attain their peaks at the top-level of the pipe ($z/D \approx 1$), which indicates the corresponding high-velocity fluctuations due to enhanced turbulence mixing at that level. Turbulence intensities are declining with a further rise in $\overline{z}$ for $z/D > 1$. The peaks of turbulence intensities show increasing trends in the near-wake region and decreasing patterns in the far-wake region along the streamwise direction, $\hat{x}$. These patterns are attributed to the enhanced turbulence in the former region and the attenuated turbulence in the latter region. Below the top level of the pipe, $z/D \leq 1$, the turbulence intensities dampened with a fall in $\overline{z}$ due to a reduction in the turbulence mixing with a decline in $\overline{z}$. In the free-surface region, $\overline{z} > 0.8$, turbulence intensities attained very small magnitudes and became approximately constant against $\overline{z}$. This result indicates that the free-surface region is far away from the influence of the bed and the cylinder.

Figure 11a,b display the variation of $\Delta\sigma_u/(\Delta\sigma_u)_{max}$ and $\Delta\sigma_w/(\Delta\sigma_w)_{max}$, respectively, against z/z_2 for Run 1, Run 2, Run 3, and Run 4 in the wall-wake region of the circular pipe, depicting the self-preserving characteristics of the turbulence intensities distributions. The self-preservation of the wall-wake is also evaluated based upon the collapse of the turbulence intensities deficit profiles. The maximum turbulence intensities deficits, $(\Delta\sigma_u)_{max}$ and $(\Delta\sigma_w)_{max}$, are used as velocity scales, respectively, for $\Delta\sigma_u$ and $\Delta\sigma_w$, and the half RSS profile width, z_2, is taken as the wall-normal length scale. The turbulence intensities deficits, $\Delta\sigma_u$ and $\Delta\sigma_w$, are calculated as the difference between the downstream wall-wake turbulence intensities at a particular elevation, z, and upstream undisturbed turbulence intensities at the same elevation. The turbulence intensities deficits, $\Delta\sigma_u(z)$ and $\Delta\sigma_w(z)$, at a particular elevation, z, can be written as $\Delta\sigma_u\ (z) = \sigma_u(z)_{d/s} - \sigma_u(z)_{u/s}$ and $\Delta\sigma_u\ (z) = \sigma_u(z)_{d/s} - \sigma_u(z)_{u/s}$, respectively. Here, $\sigma_u(z)_{u/s}$ and $\sigma_w(z)_{u/s}$ are the upstream undisturbed turbulence intensities in streamwise and wall-normal directions, respectively, at an elevation, z, while $\sigma_u(z)_{d/s}$ and $\sigma_w(z)_{d/s}$ are turbulence intensities in streamwise and wall-normal directions, respectively, in the wall-wake region of the pipe at particular $\hat{x}$ at the same elevation. The turbulence intensities deficit profiles collapse on a narrow band when scaled by these characteristic scales of velocity and length, representing that the wall-wake region of the pipe is self-preserving in nature. The self-preserving behaviour of the

turbulence intensities distributions is found to be independent of approach flow conditions. All of the turbulence intensities profiles show good collapse with the streamwise distance, $\hat{x}$, for the wall-normal domain of the study, $z/D < 2$.

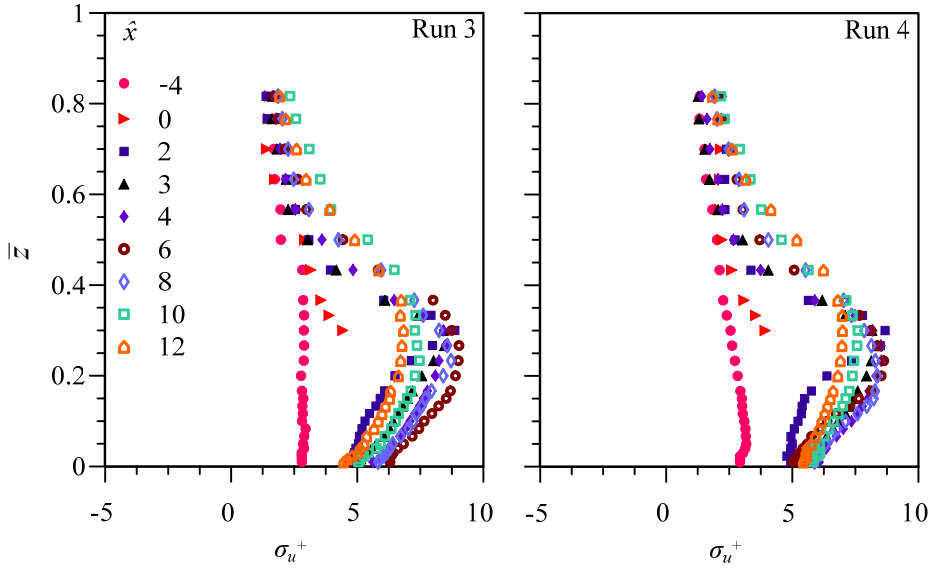

Figure 9. Wall-normal profiles of non-dimensional streamwise turbulence intensity, ${\sigma_u}^+$ in the wake region of the pipe at different streamwise locations, $\hat{x}$, for Run 3 and Run 4.

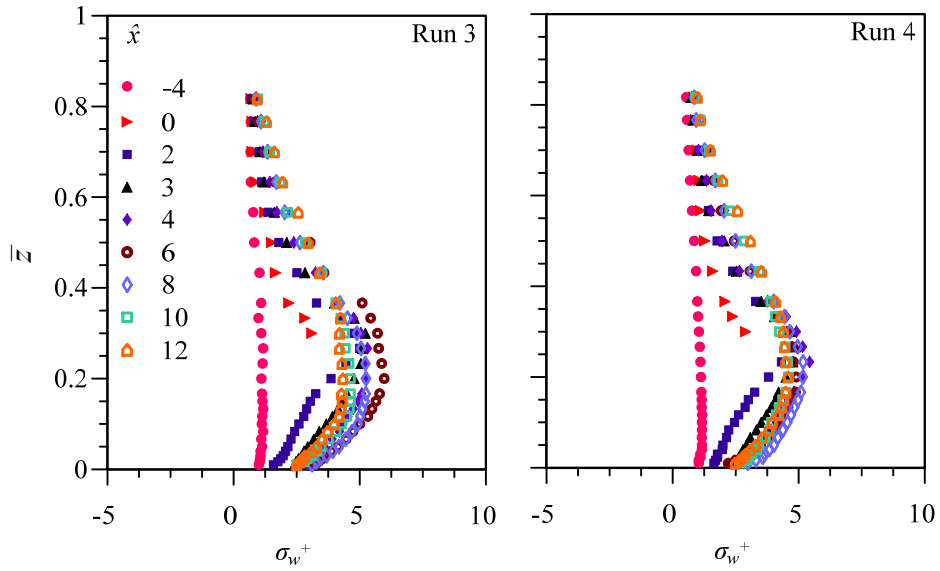

Figure 10. Wall-normal profiles of non-dimensional wall-normal turbulence intensity, ${\sigma_w}^+$, in the wake region of the pipe at different streamwise locations, $\hat{x}$, for Run 3 and Run 4.

The streamwise decay of non-dimensional maximum turbulence intensities deficits, $-(\Delta\sigma_u)_{max}/u_*$ and $-(\Delta\sigma_w)_{max}/u_*$ for Run 1, Run 2, Run 3, and Run 4 are illustrated in Figure 11c,d. The approach flow shear velocity, u_*, is taken as the velocity scale to normalize the maximum turbulence intensities deficits, $-(\Delta\sigma_u)_{max}$ and $-(\Delta\sigma_w)_{max}$. It is observed from Figure 11c that the maximum streamwise turbulence intensity deficit decreases slowly with $\hat{x}$. However, the maximum wall-normal turbulence intensity deficit increases in the beginning and attaining maximum value at $\hat{x} = 6$, and after that, it falls with a further rise in the streamwise distance, as is visible from Figure 11d.

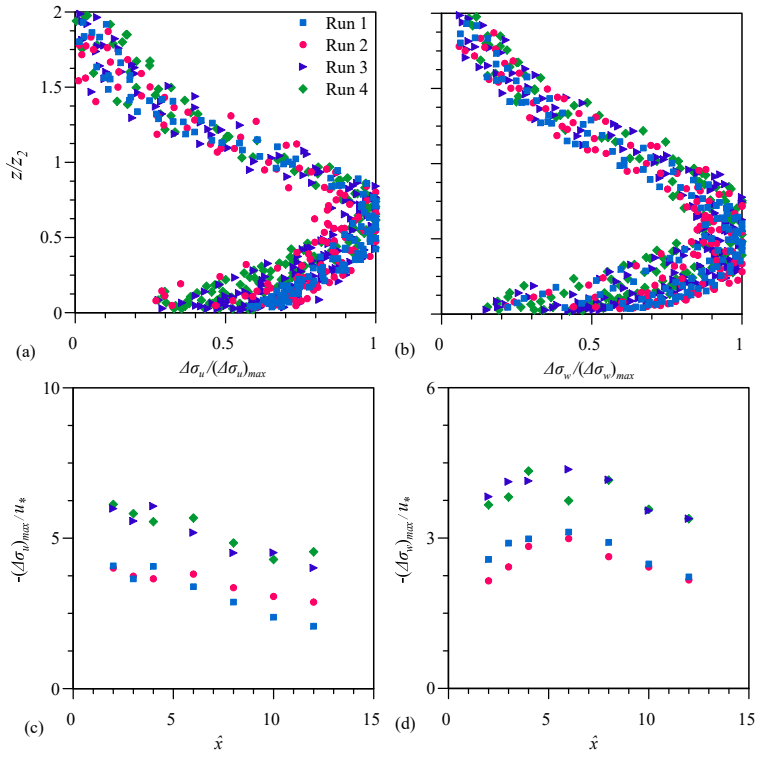

Figure 11. Self- preservation analysis of turbulence intensities in the wall-wake region of the circular pipe for Run 1, Run 2, Run 3, and Run 4: (**a**) variation of $\Delta\sigma_u/(\Delta\sigma_u)_{max}$ against z/z_2, depicting the self-preservation in streamwise turbulence intensity deficit ($\Delta\sigma_u$) distribution; (**b**) variation of $\Delta\sigma_w/(\Delta\sigma_w)_{max}$ against z/z_2, depicting the self-preservation in wall-normal turbulence intensity deficit ($\Delta\sigma_w$) distribution; (**c**) streamwise decay of non-dimensional maximum streamwise turbulence intensity deficit,$-(\Delta\sigma_u)_{max}/u_*$; (**d**) streamwise decay of non-dimensional maximum wall-normal turbulence intensity deficit,$-(\Delta\sigma_w)_{max}/u_*$.

The third-order correlations give valuable information about the fluxes and diffusion of the Reynolds normal stresses (RNSs) [25]. To be precise, the effective response of the bursting events can also be determined by the third-order correlations [24]. The third-order correlations (M_{jk}) are expressed as $M_{jk} = \overline{\hat{u}'^j \hat{w}'^k}$ where $j + k = 3$, $\hat{u} = u'/\left(\overline{u'u'}\right)^{0.5}$, and $\hat{w} = w'/\left(\overline{w'w'}\right)^{0.5}$. The third-order correlations can be categorized into four categories, namely: flux of streamwise RNS in the flow direction, $M_{30} = \overline{\hat{u}^3} = \overline{u'^3}/\left(\overline{u'u'}\right)^{3/2}$; flux of the wall-normal RNS in the wall-normal direction, $M_{03} = \overline{\hat{w}^3} = \overline{w'^3}/\left(\overline{w'w'}\right)^{3/2}$; diffusion of streamwise RNS in wall-normal direction, $M_{21} = \overline{\hat{u}^2\hat{w}} = \overline{u'^2w'}/\left(\overline{u'u'}\right)\left(\overline{w'w'}\right)^{1/2}$; and diffusion of wall-normal RNS in the streamwise direction, $M_{12} = \overline{\hat{u}\hat{w}^2} = \overline{u'w'^2}/\left(\overline{u'u'}\right)^{1/2}\left(\overline{w'w'}\right)$. The wall-normal profiles of the third-order correlations, M_{jk}, in the wake region of the pipe at different $\hat{x}$ for Run 3 and Run 4 are illustrated in Figure 12.

A closer look at Figure 12 demonstrates that at the upstream undisturbed location ($\hat{x} = -4$), M_{30} and M_{12} begin with an insignificantly small negative value in the near-bed region and then consistently increased (negative magnitude) with a rise in $\bar{z}$ for both runs which are typical of turbulent shear flows over rigid surfaces [22]. Although, in the wake region, M_{30} and M_{12} start with small positive values, M_{30} and M_{12} decrease with a rise in the wall-normal distance from the bed and change their signs near the top level of the cylinder for both the runs. With a further rise in $\bar{z}$, their negative magnitude increase sharply and attain their negative peaks at $\bar{z} \approx 0.4$. After that, negative magnitudes of M_{30}

and M_{12} decrease gradually with $\bar{z}$ and become almost invariant of $\bar{z}$ in the free surface zone. It is noteworthy that the variation of M_{03} and M_{21} occur very similarly to M_{30} and M_{12}, however with the opposite signs. Unlike M_{30} and M_{12} distributions, M_{03} and M_{21} begin at bed with small negative values in the wake region. The negative magnitudes of M_{03} and M_{21} decrease with a further rise in $\bar{z}$, and change their signs at $z \approx$ D. After that, the value of M_{03} and M_{21} increase gradually with a rise in the vertical distance from the bed and attain peaks and decrease with a further rise in z, and become almost constant and invariant of z in the near free surface region. The positive and negative values of M_{30} and M_{03}, respectively, reveal that the downstream flux of streamwise RNS was associated with a downward flux of wall-normal RNS in the near-bed region, while the positive and negative values of M_{12} and M_{21} indicate the downstream advection of streamwise RNS and downward advection of wall-normal RNS in the near-bed region. Therefore, it can be understood that the dominance of sweep events in the near-bed region makes M_{30} and M_{12} to be positive and M_{03} and M_{21} to be negative. The negative values of M_{30} and M_{12} and positive values of M_{03} and M_{21} away from the boundary indicates the influence of the ejection events in the disturbed outer layer region. The sweep event represents a high-speed fluid parcel rushed towards the bed and is mainly responsible for bed mobility. From overall observations, it is clear that the enhanced contribution of M_{30} (positive) and M_{03} (negative) in the downstream region of the pipe reveal an intense momentum exchange in the near-bed region.

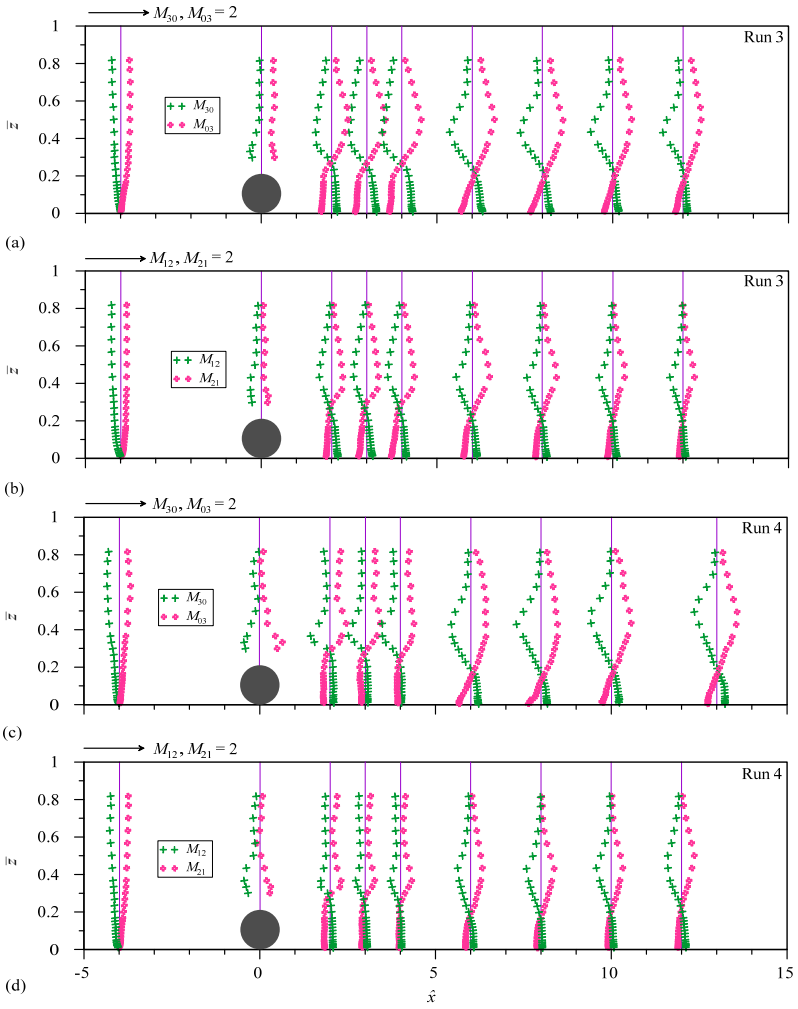

Figure 12. The wall-normal profiles of the third-order correlations, M_{ij} in the wake region of the pipe at different $\hat{x}$ for Run 3: (**a**) M_{30} and M_{03}, (**b**) M_{21} and M_{12}; and for Run 4: (**c**) M_{30} and M_{03}, and (**d**) M_{21} and M_{12}.

4. Conclusions

The significance of this research is that it analyze the self-preserving characteristics of turbulent flow statistics in the wall-wake of the bed-mounted horizontal pipe at different hydraulic and physical conditions. Additionally, the streamwise variations of the wall-normal profiles of the third-order correlations were evaluated. The self-preserving characteristics of the wall-wake region of the pipe were evaluated based on the collapse of the non-dimensional wall-normal profiles of velocity deficit $\Delta u/(\Delta u)_{max}$, non-dimensional RSS deficit $\Delta\tau_{uw}/(\Delta\tau_{uw})_{max}$, non-dimensional streamwise turbulence intensity deficit $\Delta\sigma_u/(\Delta\sigma_u)_{max}$, and non-dimensional wall-normal turbulence intensity deficit $\Delta\sigma_w/(\Delta\sigma_w)_{max}$ at various streamwise distances, $\hat{x}$. The velocity deficit, RSS deficit, and turbulence intensities deficit distributions exhibited good collapse under this scaling, demonstrating the self-preserving behaviour of the mean and turbulent flow field. The variation of the half velocity profile width, z_1, and half RSS profile width, z_2, with streamwise distance indicated the expansion or contraction of the wake region in the streamwise direction. Therefore, it is clear that the wall-wake flow of a bed-mounted horizontal circular pipe shows the self-preserving behaviour under different inflow conditions. The findings of this study will be useful for the validation and improvement of numerical models, and quick prediction of the wall-wake flows for evaluation of self-preservation. Finally, the important findings of the study are enumerated as follows.

1. The recirculation region is stretched up to $\hat{x} = 7.4$, which is more than the value found in the existing literature on the topic.
2. The self-preserving characteristics such as turbulence intensities and Reynolds shear stresses start from $\hat{x} = 3$ and the flow field is found to be not yet recovered even at $\hat{x} = 12$.
3. In the wall normal direction, self-preserving of velocity profiles, RSS profiles, and turbulence intensities is found for $z/D < 2$ and self preservation is not found for $z/D > 2$.
4. The points of inflection ($d^2\overline{u}/dz^2 = 0$) in the individual u^+ profiles are observed near the top level of the pipe, $z/D \approx 1$. Therefore, RSS and turbulence intensities are attaining their peaks at $z/D \approx 1$.
5. The velocity deficit profile exhibits a single peak in its distribution at $z/z_1 \approx 0.25$, the RSS deficit profiles display a single peak at $z/z_1 \approx 0.6$, and the turbulence intensities deficit profiles display a single peak at $z/z_1 \approx 0.8$.
6. The streamwise decay of peak values of non-dimensional velocity defect, non-dimensional RSS defect, and non-dimensional turbulence intensity defect indicates recovery of flow.
7. The half RSS defect profile width, half velocity defect profile width, and the half turbulence defect profile width grow in the streamwise direction, which indicates weaning of the wake strength.
8. In the wake region, third-order moments M_{03} and M_{21} begin at the bed with small negative values, whereas M_{30} and M_{12} begin at the bed with small positive values. They change their signs at $z \approx$ D, which proves that sweep events are dominant below the level of the cylinder and ejection events are dominant above the level of the cylinder.

Author Contributions: K.D.: writing—original draft preparation, writing—review and editing, and data curation; P.R.H.: writing—original draft preparation, writing—review and editing, funding acquisition, project administration, data curation, and supervision; R.B.: writing—review and editing, data curation; J.H.P.: writing—review and editing, and data curation. All authors contributed to the work. All authors have read and agreed to the published version of the manuscript.

Funding: This research received no external funding.

Institutional Review Board Statement: Not applicable.

Informed Consent Statement: Not applicable.

Data Availability Statement: The data presented in this study are available on reasonable request from the corresponding author.

Conflicts of Interest: The authors declare no conflict of interest.

References

1. Djeridi, H.; Braza, M.; Perrin, R.; Harran, G.; Cid, E.; Cazin, S. Near-wake turbulence properties around a circular cylinder at high Reynolds number. *Flow Turbul. Combust.* **2003**, *71*, 19–34. [CrossRef]
2. Konstantinidis, E.; Balabani, S.; Yianneskis, M. The effect of flow perturbations on the near wake characteristics of a circular cylinder. *J. Fluids Struct.* **2003**, *18*, 367–386. [CrossRef]
3. Braza, M.; Perrin, R.; Hoarau, Y. Turbulence properties in the cylinder wake at high Reynolds numbers. *J. Fluids Struct.* **2006**, *22*, 757–771. [CrossRef]
4. Akoz, M.S. Flow structures downstream of the horizontal cylinder laid on a plane surface. *Proc. Inst. Mech. Eng. Part C J. Mech. Eng. Sci.* **2009**, *223*, 397–413. [CrossRef]
5. Akoz, M.S.; Kirkgoz, M.S. Numerical and experimental analyses of the flow around a horizontal wall-mounted circular cylinder. *Trans. Can. Soc. Mech. Eng.* **2009**, *33*, 189–215. [CrossRef]
6. Devi, K.; Hanmaiahgari, P.R. Experimental analysis of turbulent open channel flow in the near-wake region of a surface-mounted horizontal circular cylinder. In *River Flow 2020: Proceedings of the 10th Conference on Fluvial Hydraulics, Delft, The Netherlands, 7–10 July 2020*; CRC: Boca Raton, FL, USA, 2020; pp. 194–202.
7. Devi, K.; Hanmaiahgari, P.R.; Balachandar, R.; Pu, J.H. A Comparative Study between Sand- and Gravel-Bed Open Channel Flows in the Wake Region of a Bed-Mounted Horizontal Cylinder. *Fluids* **2021**, *6*, 239. [CrossRef]
8. Balachandar, R.; Ramachandran, S.; Tachie, M.F. Characteristics of shallow turbulent near wakes at low Reynolds numbers. *J. Fluids Eng. Trans. ASME Eng.* **2000**, *122*, 302–308. [CrossRef]
9. Balachandar, R.; Tachie, M.F.; Chu, V.H. Concentration profiles in shallow turbulent wakes. *J. Fluids Eng. Trans. ASME* **1999**, *121*, 34–43. [CrossRef]
10. Nasif, G.; Barron, R.M.; Balachandar, R. DES evaluation of near-wake characteristics in a shallow flow. *J. Fluids Struct.* **2014**, *45*, 153–163. [CrossRef]
11. Akilli, H.; Rockwell, D. Vortex formation from a cylinder in shallow water. *Phys. Fluids* **2002**, *14*, 2957–2967. [CrossRef]
12. Singha, A.; Balachandar, R. Structure of wake of a sharp-edged bluff body in a shallow channel flow. *J. Fluids Struct.* **2011**, *27*, 233–249. [CrossRef]
13. Townsend, A. Measurements in the turbulent wake of a cylinder. *Proc. R. Soc. Lond. Ser. A Math. Phys. Sci.* **1947**, *190*, 551–561. [CrossRef]
14. Townsend, A. Momentum and energy diffusion in the turbulent wake of a cylinder. *Proc. R. Soc. Lond. Ser. A Math. Phys. Sci.* **1949**, *197*, 124–140. [CrossRef]
15. Maji, S.; Hanmaiahgari, P.R.; Balachandar, R.; Pu, J.H.; Ricardo, A.M.; Ferreira, R.M. A Review on Hydrodynamics of Free Surface Flows in Emergent Vegetated Channels. *Water* **2020**, *12*, 1218. [CrossRef]
16. Sadeque, M.F.; Rajaratnam, N.; Loewen, M.R. Shallow turbulent wakes behind bed-mounted cylinders in open channels. *J. Hydraul. Res.* **2009**, *47*, 727–743. [CrossRef]
17. Tachie, M.F.; Balachandar, R. Shallow wakes generated on smooth and rough surfaces. *Exp. Fluids* **2001**, *30*, 467–474. [CrossRef]
18. Maji, S.; Pal, D.; Hanmaiahgari, P.R.; Gupta, U.P. Hydrodynamics and turbulence in emergent and sparsely vegetated open channel flow. *Environ. Fluid Mech.* **2017**, *17*, 853–877. [CrossRef]
19. Pu, J.H. Velocity Profile and Turbulence Structure Measurement Corrections for Sediment Transport-Induced Water-Worked Bed. *Fluids* **2021**, *6*, 86. [CrossRef]
20. Goring, D.G.; Nikora, V.I. Despiking Acoustic Doppler Velocimeter Data. *J. Hydraul. Eng.* **2002**, *128*, 117–126. [CrossRef]
21. Wahl, T.L. Discussion of "Despiking Acoustic Doppler Velocimeter Data" by Derek G. Goring and Vladimir I. Nikora. *J. Hydraul. Eng.* **2003**, *129*, 484–487. [CrossRef]
22. Mori, N.; Suzuki, T.; Kakuno, S. Noise of Acoustic Doppler Velocimeter Data in Bubbly Flows. *J. Eng. Mech.* **2007**, *133*, 122–125. [CrossRef]
23. Chanson, H.; Trevethan, M.; Aoki, S. Acoustic Doppler velocimetry (ADV) in small estuary: Field experience and signal post-processing. *Flow Meas. Instrum.* **2008**, *19*, 307–313. [CrossRef]
24. Nezu, I.; Nakagawa, H. *Turbulence in Open Channel Flows*; IAHR: Rotterdam, The Netherlands, 1993; ISBN 9054101180.
25. Gad-el-Hak, M.; Bandyopadhyay, P.R. Reynolds Number Effects in Wall-Bounded Turbulent Flows. *Appl. Mech. Rev.* **1994**, *47*, 307–365. [CrossRef]